

Vitrification and increase of basicity in between ice I_h crystals in rapidly frozen dilute NaCl aqueous solutions

Cite as: J. Chem. Phys. 151, 014503 (2019); <https://doi.org/10.1063/1.5100852>

Submitted: 21 April 2019 . Accepted: 31 May 2019 . Published Online: 03 July 2019

Kamila Imrichová , Lukáš Veselý , Tobias M. Gasser , Thomas Loerting , Vilém Neděla , and Dominik Heger 



[View Online](#)



[Export Citation](#)



[CrossMark](#)

ARTICLES YOU MAY BE INTERESTED IN

Transitions in pressure-amorphized clathrate hydrates akin to those of amorphous ices
The Journal of Chemical Physics 151, 014502 (2019); <https://doi.org/10.1063/1.5096981>

Is water one liquid or two?

The Journal of Chemical Physics 150, 234503 (2019); <https://doi.org/10.1063/1.5096460>

Amorphous and crystalline ices studied by dielectric spectroscopy

The Journal of Chemical Physics 150, 244501 (2019); <https://doi.org/10.1063/1.5100785>

[Submit Today](#)

**The Journal
of Chemical Physics**

The Emerging Investigators Special Collection and Awards
Recognizing the excellent work of early career researchers!

Vitrification and increase of basicity in between ice I_h crystals in rapidly frozen dilute NaCl aqueous solutions

Cite as: J. Chem. Phys. 151, 014503 (2019); doi: 10.1063/1.5100852

Submitted: 21 April 2019 • Accepted: 31 May 2019 •

Published Online: 3 July 2019



Kamila Imrichová,^{1,2} Lukáš Veselý,¹ Tobias M. Gasser,³ Thomas Loerting,³ Vilém Neděla,² and Dominik Heger^{1,a)}

AFFILIATIONS

¹ Department of Chemistry, Faculty of Science, Masaryk University, Kamenice 5, 62500 Brno, Czech Republic

² Institute of Scientific Instruments of the ASCR, v.v.i., Královopolská 147, 61264 Brno, Czech Republic

³ Institute of Physical Chemistry, University of Innsbruck, A-6020 Innsbruck, Austria

Note: This paper is part of a JCP Special Topic on Chemical Physics of Supercooled Water.

a) Author to whom correspondence should be addressed: hegerd@chemi.muni.cz

ABSTRACT

The freezing of ionic aqueous solutions is common in both nature and human-conducted cryopreservation. The cooling rate and the dimensions constraining the solution are known to fundamentally influence the physicochemical characteristics of the sample, including the extent of vitrification, morphology, and distribution of ions. The presence of some salts in an aqueous solution often suppresses the ice crystallization, allowing bulk vitrification during relatively slow cooling. Such a process, however, does not occur in NaCl solutions, previously observed to vitrify only under hyperquenching and/or in sub-micrometric confinements. This work demonstrates that, at freezing rates of $\geq 100\text{ K min}^{-1}$, crystallized ice I_h expels the freeze-concentrated solution onto the surfaces of the crystals, forming lamellae and veins to produce glass, besides eutectic crystallization. The vitrification covers ($6.8\% \pm 0.6\%$) and ($17.9\% \pm 1.5\%$) of the total eutectic content in 0.06M and 3.4 mM solutions, respectively. The vitrified solution shows a glass-to-liquid transition succeeded by cold crystallization of NaCl · 2H₂O during heating via differential scanning calorimetry. We establish that ice crystallization is accompanied by increased basicity in freeze-concentrated solutions, reflecting preferential incorporation of chloride anions over sodium cations into the ice. After the sample is heated above the glass transition temperature, the acidity gradually returns towards the original value. The morphology of the samples is visualized with an environmental scanning electron microscope. Generally, the method of vitrifying the freeze-concentrated solution in between the ice I_h crystals via fast cooling can be considered a facile route towards information on vitrified solutions.

Published under license by AIP Publishing. <https://doi.org/10.1063/1.5100852>

INTRODUCTION

Water is known to form 17 crystalline and three amorphous solids depending on the temperature and pressure.^{1,2} While amorphous solid water constitutes probably the most abundant form of ice in space,^{3,4} the hexagonal crystalline modification (I_h) is characteristic of the Earth, considering the prevailing temperatures and pressures.⁵ For this reason, ice I_h is widely studied, whereas the other modifications have drawn proportionally less attention. Despite the intensive research efforts and importance of the problem for many fields of science, understanding the

various facets of water ice(s) behavior remains a matter of ongoing debate.^{6–8}

Vitrification of aqueous solutions plays a major role in the natural environment, where vitrified solutions are observed to behave very differently from the supercooled or crystallized ones.^{9,10} The process has also attracted substantial interest within the cryomicroscopy community in which the preparation of biochemical samples in an aqueous glassy matrix opened a large potential for detailed investigation at the molecular scale.^{11–14} This branch of microscopy was established only through Erwin Mayer's hyperquenching method, yielding fully vitrified micrometer-sized

droplets of pure water by very rapid cooling (10^7 K s^{-1}).^{15,16} Water is considered a poor glass forming material as the slower cooling rates lead to the formation of crystalline ice. One of the most striking differences between ice I_h on the one hand and liquid water and amorphous ice on the other consists in the tolerance to impurities: I_h expels nearly all such substances to its boundaries,^{17–19} whereas a solution can be hyperquenched to the amorphous phase so fast that the impurities vitrify close to their original positions.²⁰

The presence of inorganic salts offers an attractive route to studying the amorphous forms of aqueous solutions, as, compared to pure water, these salts lower the homogeneous crystallization temperature and (at high concentrations) increase the glass transition temperature; thus, the ice crystallization is often suppressed.^{6,21–23} All alkali chloride solutions nevertheless exhibit a non-glass forming region, where standard cooling rates of up to about 1000 K min^{-1} are not sufficient to facilitate vitrification.^{23–25} Such a scheme usually accompanies dilute solutions, the ones far below the eutectic concentration. Around the eutectic concentration, LiCl solutions are easier to vitrify than the NaCl (and other alkali chloride) ones, and even the cooling rate of 0.33 K min^{-1} may suffice for full vitrification.^{21,24–26} Except for the hyperquenching study by Hallbrucker and Mayer,²⁷ to our knowledge, however, vitrification in a bulk solution of NaCl has not been reported thus far. The cooling rate of 10^4 K s^{-1} was needed to produce a 90% vitrified solution with $20 \mu\text{m}$ droplets; the remaining 10% was formed by ice I_h.²⁶

At present, the only viable alternative to the preparation of fully vitrified salty aqueous solutions relies on cooling solutions in confined volumes, strongly impeding the crystallization of ice. Such a condition was experimentally obtained either via emulsions²⁸ or by ensuring confinement in micro- or nanoporous materials.^{6,29} Freezing NaCl solutions in an emulsion allowed glass transition temperature observation exclusively for pressures above 100 MPa .²¹ The hyperquenching of NaCl aqueous solutions in microdroplets yielded fully vitrified glass solutions at cooling rates of about 10^7 K s^{-1} ,²⁷ and largely vitrified solutions at 10^4 K s^{-1} .³⁰ In the latter case, the amorphous structure was found to resemble the structure of high density amorphous ice even at atmospheric pressure. Homogeneously nucleated ice from microscopic droplets in an oil emulsion revealed a relationship between NaCl concentration (and thus the homogeneous nucleation temperature) and preference for the formation of I_c crystals.³¹ Compared to ammonium hydrogen-sulfates, NaCl has not been proven to produce an amorphous phase in microemulsions.²⁸ Partial vitrification of an aqueous solution in nanometer-wide capillaries was nevertheless demonstrated recently.³²

The freeze concentrated solution (FCS) threading the ice crystals creates a specific and hitherto not fully described medium whose behavior is of utmost importance in various fields, including geological, atmospheric, life, and pharmaceutical sciences. To date, FCSs have been examined via microscopy^{33–36} and also characterized spectroscopically^{37–40} and calorimetrically,^{41–43} applying numerous systems at various temperatures within diverse fields. The FCS was found to behave distinctly from the impurities deposited from the gaseous phase.^{44,45} The impurities segregated from the ice either create pools or fill the pores between two ice crystals on the surfaces; where, however, three ice grains meet in the ice bulk volume, triple junction tubes (also termed veins) may emerge.^{36,46} The diameters

of the observed venous filaments formed by deep freezing of NaCl FCSs in between partly sublimed ice I_h crystals varied from 0.2 to $2.5 \mu\text{m}$.^{47,48}

The solutes in FCSs can experience acidity changes as compared to the original solution. We are aware of three reasons for acidity jumps during freezing: (1) a trivial increase in the concentrations through a decrease in the volume,⁴⁹ (2) partial crystallization of the salts,^{50–52} and (3) acidity changes induced by an unequal distribution of the ions present between the ice lattice and FCS.^{49,53,54} The method utilizing sulfonephthalein indicators to evaluate frozen and lyophilized solutions was developed independently by Shalaev, Zografi *et al.*⁵⁵ and our group;⁴⁹ in this context, several successful applications to various systems were described.^{50,53,56–59} Recently, the effects of a trivial concentration increase were shown to explain very precisely the observed changes in the protonation extent for frozen solutions of acids and bases.⁶⁰

In this work, sodium chloride was chosen to represent an ionic compound in an aqueous solution; NaCl is commonly contained in natural waters and also embodies a typical constituent in buffers used for maintaining the ionic strength and thus the stability of biomolecules.¹¹² Seawater, amounting to 96.5% of water on the Earth,⁶¹ comprises a considerable volume of dissolved salts, with Na⁺ and Cl⁻ ions being major components. Salty ice is also common in nature,^{62,63} and a portion of the sea salt aerosols freeze during winter.^{9,64–67}

This article elucidates the processes that accompany the freezing of NaCl solutions. We applied differential scanning calorimetry (DSC), the pH indicator method, and environmental scanning electron microscopy (ESEM) to establish that ice I_h is threaded by freeze concentrated eutectic solutions which can crystallize or partly turn into glass, depending on the cooling rate. The processes are accompanied by not only the release of heat characteristic of crystallization and vitrification but also changes of acidity.

METHODS

The 0.06M and 3.42 mM NaCl samples were prepared by dissolving the corresponding amount of the salt in demineralized water. For the spectroscopic measurements, one of the acid-base indicators was added to the 0.06M NaCl solution. The concentration of the bromocresol purple (BCP) indicator in the 0.06M NaCl solution was $3.70 \times 10^{-6} \text{ M}$, and the relevant concentration of cresol red (CR) corresponded to $7.42 \times 10^{-6} \text{ M}$.

Differential scanning calorimetry

To perform the calorimetric analysis, we used a Perkin Elmer DSC 8000 differential scanning calorimeter. Before the measurements, the liquid sample was sealed into aluminum DSC crucibles and weighted to normalize the measured thermograph. Within the actual procedure, the sample was first cooled down in the temperature range between 290 and 100 K at three different rates, namely, 100, 20, and 5 K/min. Subsequently, heating from 100 to 290 K was carried out, using the rate of 30 K/min. The thermographs were normalized by the solution weights; thus, the ordinates are shown in units of mW mg^{-1} , with the exothermic events oriented downwards. In the cold loading procedure, we prepared the frozen sample by spraying the microdroplets (herein also termed “ice spheres”) into

a vessel with liquid nitrogen. The ice spheres were then loaded into the aluminum crucibles, and these were manually closed under the liquid nitrogen. The weight of the solution was not determined for ice spheres. A baseline correction was needed in the DSC scans. The straight line with a slope of the linear part of the thermograph signal between 120 K and 250 K was subtracted from the measured scan to correct the sloping baseline and to enhance the visualization of the changes measured in the heat flow.

Spectrophotometric measurements

The measurements were performed utilizing an Agilent Cary 5000 UV-Vis-NIR spectrophotometer with an Agilent Internal DRA 2500 integrating sphere. The samples were measured in plastic cuvettes sized $1 \times 1 \text{ cm}^2$ (Brand UV cuvettes, macro, Cat. No. 7591 70). The cooling process consisted in immersing the sample into boiling liquid nitrogen at 77 K; the temperature was monitored using a Pt100 thermometer. The absorption spectra of the samples were measured in various temperature intervals, with the temperature gradually increasing. After measurement in the low temperature interval (84 K–137 K), we tempered the sample in a precooled bath at 210 K; the temperature was reached via dosing dry ice into ethanol.

To facilitate the spectroscopic investigation of the acidity change in the frozen solution, one of the following two acid-base indicators was used: 4,4'-(1,1-dioxido-3H-2,1-benzoxathiole-3,3-diyl)-bis(2-bromo-6-methylphenol), also called bromocresol purple (BCP), and 2-[bis(4-hydroxy-3-methylphenyl)-methyliumyl] benzenesulfonate, otherwise known as cresol red (CR). Both substances belong to the class of sulfonephthaliein dyes.

BCP can exist in two spectroscopically well-defined forms between pH 4 and 10. The more acidic form B exhibits the absorption maximum of λ_{\max} 432 nm; the basic form, C, is then characterized by λ_{\max} 589 nm. The value of pK_a was established to be 6.47 at 303 K; an increase is observable with decreasing temperature, amounting to 6.51 at 293 K and 6.56 at 283 K at zero ionic strength.^{68,69}

Cresol red exists in three forms, depending on the pH. All of these, A, B, and C, have absorption bands in the visible region, with λ_{\max} at 518, 434, and 573 nm, respectively.¹¹³ The doubly protonated form, A, represents a very acidic environment; the mono-protonated variant, B, is associated with neutral conditions; and the deprotonated modification, C, exists in a basic environment as the pK_1^1 equals 1×10^{70} and the pK_2^2 equals 8.15.⁷¹ The CR forms exhibit a zwitterion structure, and a prolonged conjugated system is responsible for their colors.⁷²

Hammett acidity function H_{2-}

The pH scale for describing acidity finds use mostly in dilute aqueous solutions; hence, H_{2-} was employed to quantify the acidity at a wide scale⁷³ in mixtures of solutions,⁷⁴ lyophiles,⁷⁵ and frozen solutions.^{50,53} The notation was established to specify the protonation equilibrium of polyprotic acids in such a manner that the subscript of the H specifies the charge of the base in question.⁷⁵ In both applied indicators, the stronger bases (denoted as the form C) have the charge 2 $-$; we therefore refer to the Hammett acidity function H_{2-} . When computing the H_{2-} values, we fitted the spectra of the

pure forms into the measured spectra of the frozen NaCl solutions, with the relative abundances of the forms B and C denoted as c_B and c_C , respectively.

The H_{2-} values were computed using the formula

$$H_{2-} = pK_a + \log \frac{c_C}{c_B}$$

The absorption spectra of the pure forms in the frozen state (B and C, respectively) were obtained from the 0.06M NaCl frozen solutions at the initial room temperature (RT) pHs of 4.16 and 10.00 in the BCP and 4.50 and 12.1 in the CR. When measuring the BCP-dyed samples at RT and in the frozen state, we utilized the pK_a values of 6.51 and 6.56, respectively; with the CR, the applied value corresponded to 8.15 in both conditions. The pK_a values in an aqueous solution may differ from the frozen solution values; however, H_{2-} values can be used for comparison in relative terms.⁷⁶

ESEM

An AQUASEM II environmental scanning electron microscope, namely, a Tescan VEGA device custom modified at the Institute of Scientific Instruments of the Czech Academy of Sciences, was used for observing the frozen 0.06M NaCl samples.⁷⁷ The microscope is capable of representing wet, non-conducting samples under a pressure of up to 2000 Pa (20 mbar) and a temperature down to 223 K. The electron beam energy corresponded to 20 keV, the dwell time was set to 61 μs (768 \times 768 pixels), and the beam current equaled 80 pA. During the experiments, the air and water vapor pressures were 300 Pa (3 mbar) and 0 Pa, respectively. We utilized a specially built scintillation counter to detect the backscattered electrons, and the topography of the sample was investigated with an ionization detector of secondary electrons.⁷⁸ The cuvettes and solution (0.06M NaCl) were the same as those employed for the acidity assessment. We examined microscopically a piece of ice crystal from a distance of approximately 0.5 cm under the sample surface, on the Peltier stage precooled to 223 K.

RESULTS

Differential scanning calorimetry

Cooling the 0.06M NaCl solution

The first exothermic peaks, observed during cooling the aqueous solution of 0.06M NaCl at the rates of 100, 20, and 5 K min $^{-1}$ and the onset temperatures of 253, 257, and 266 K, respectively, represent the formation of I_h crystals (Fig. 1). As the total heat flux is proportional to the scan rate, the areas of the indicated peaks are larger with faster cooling. Moreover, the temperatures at which the hexagonal ice freezing starts differ for each scan rate; the faster the cooling rate, the lower the supercooling temperature reachable. The next exothermic peaks (shown in the inset of Fig. 1), detected at the onset temperatures of 233 K and 235 K for the cooling rates of 20 K min $^{-1}$ and 5 K min $^{-1}$, respectively, stand for the NaCl/water eutectic crystallization. This implies that the eutectic crystallizes from the supercooled liquid, where the supercooling amounts to about 20 K. The eutectic line in the phase diagram is located at 252 K.⁷⁹ Eutectic crystallization step is not separated from the I_h crystallization peak at the cooling rate of 100 K min $^{-1}$.

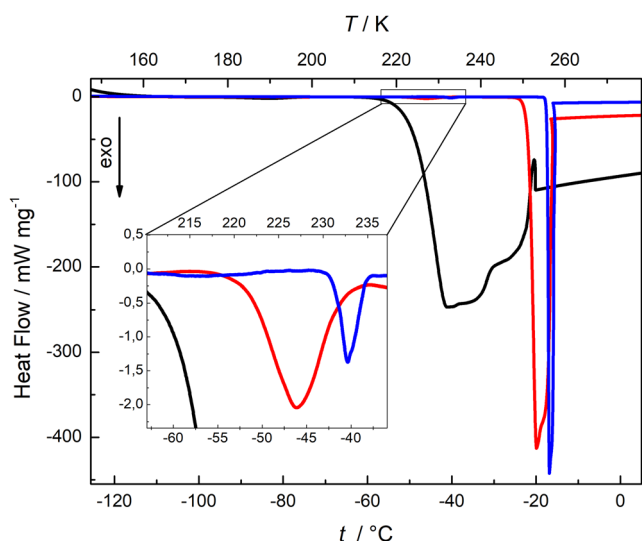


FIG. 1. The DSC cooling scan of the 0.06M NaCl solution, representing the cooling rates of 100 K min^{-1} (black), 20 K min^{-1} (red), and 5 K min^{-1} (blue). The inset is approximately 80-fold magnified.

The third thermal effect, reproducibly observable in the temperature interval of 175–205 K, is detailed in Fig. 2. While cooling down the 0.06M NaCl solution at the rate of 100 K min^{-1} , we observe a heat capacity change with the onset at $\sim 200\text{ K}$. Also at the cooling rates of 20 and 5 K min^{-1} , the heat capacity change is observed, which is shifted to a slightly higher temperature of $\sim 205\text{ K}$, but much smaller compared to the one found during the fast cooling process (the red and blue curve, respectively, in Fig. 2.). These

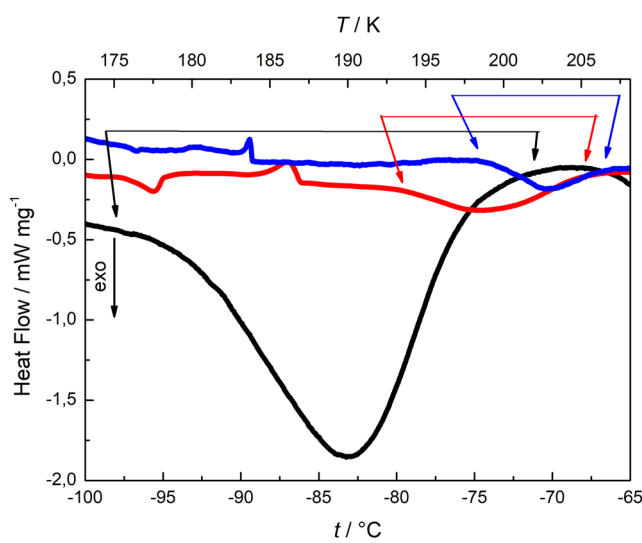


FIG. 2. The DSC cooling scan of the 0.06M NaCl solution, representing the cooling rates of 100 K min^{-1} (black), 20 K min^{-1} (red), and 5 K min^{-1} (blue). The image embodies a detail of the illustration in Fig. 1. The onsets and ends of the glass transitions are indicated by arrows having corresponding colors.

phenomena are consistent with the ones expected for the liquid-to-glass transitions of the remaining unfrozen solutions. That is, we assign the onset of the liquid-to-glass transition for the freeze-concentrated solution after freezing of ice and eutectic to be at $200\text{--}205\text{ K}$.

Cooling the 3.42 mM NaCl solution

We performed identical DSC measurements for the 3.42 mM NaCl solution. The cooling scans of the samples exhibiting lower NaCl concentrations are displayed in Figs. S1–S3 of the [supplementary material](#); the main difference from the 0.06M NaCl solution rests in the absence of the exothermic peaks of the NaCl/water eutectic crystallization (see the insets in Fig. S1 of the [supplementary material](#)). Furthermore, the heat capacity change at around 200 K is noticeable only for the 100 K min^{-1} cooling rate (Fig. S2 of the [supplementary material](#)). To facilitate comparison with the 0.06M NaCl solution, the 0.06M NaCl cooling scan (Fig. 2, the black curve) was divided by the constant $0.06/0.00342 = 17.5$ (Fig. S3 of the [supplementary material](#), the red dotted curve). The ratio accounts for the uneven concentrations in the samples. The glass transition of the remaining unfrozen solution, which is otherwise barely noticeable, is revealed to have an onset temperature of around 200 K, just like for the initially 0.06M solution (compare the location of arrows in Fig. S3 of the [supplementary material](#)). The small size of this effect is clear when considering that it pertains only to the small amount of unfrozen solution that is trapped inside ice and eutectic crystals. In future discussions, the observation of this weak signal will not constitute a basis for relevant arguments on our part. However, the better resolved signals in the heating thermograms (see below) confirm the presence of the glass transition in the cooling thermogram.

Heating the 0.06M NaCl solution

The DSC heating scans of the 0.06M NaCl solution show two major endothermic peaks (Fig. 3). The most intense peak relates to the consumed heat required for hexagonal ice melting, and the endothermic peak starting at $\sim 252\text{ K}$ corresponds to the melting of the eutectic $\text{NaCl} \cdot 2\text{H}_2\text{O}$ and ice mixture (Fig. 3, inset). The onset temperature of 252 K marked in Fig. 3 using arrow is in excellent agreement with literature data—the eutectic temperature of $\text{NaCl}/\text{H}_2\text{O}$ was determined to be 252.0 K in a previous work.⁷⁹ The heat flow after this peak does not drop back to its original value because the gradual melting of the pure ice in the NaCl brine proceeds at increasing temperature and because the heat capacity of a partly liquid sample is higher than the heat capacity of the fully crystallized sample.

The 6-fold magnification of the heating thermogram of the 0.06M NaCl solution (Fig. 4, inset) shows an exothermic peak with the minimum at $\sim 197\text{ K}$ in a sample cooled using the rate of 100 K min^{-1} (see the black curve). This peak is either minute or completely absent for samples frozen at the cooling rates of 20 and 5 K min^{-1} (the red and blue curves), respectively. The dashed gray curve in Fig. 4 indicates the differences between the thermogram measured after cooling at 100 K min^{-1} and 5 K min^{-1} (the black minus the blue curve). Thus, the dashed gray curve carries mainly information about the processes related to the glass-to-liquid transition in the NaCl solution, without an interference of the heat changes

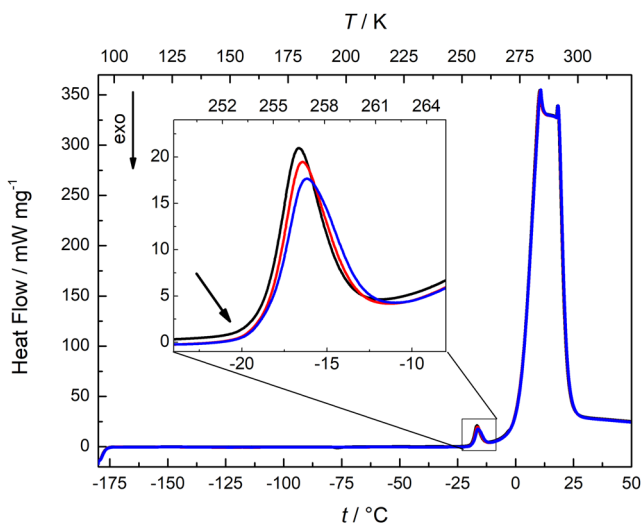


FIG. 3. The DSC heating scan (for the rate of 30 K min^{-1}) characterizing the 0.06M NaCl solution after freezing at the cooling rates of 100 K min^{-1} (black), 20 K min^{-1} (blue), and 5 K min^{-1} (red), with the NaCl/water eutectic endothermic peak at 252 K indicated by the black arrow (detailed in the inset via 100-fold magnification).

accompanying the bulk ice behavior. Importantly, a heat capacity change is clearly observable for the interval of 180 – 190 K preceding the exothermic peak. The beginning of the transition at 182 K is indicated by the black arrow in Fig. 4. For reasons outlined in the

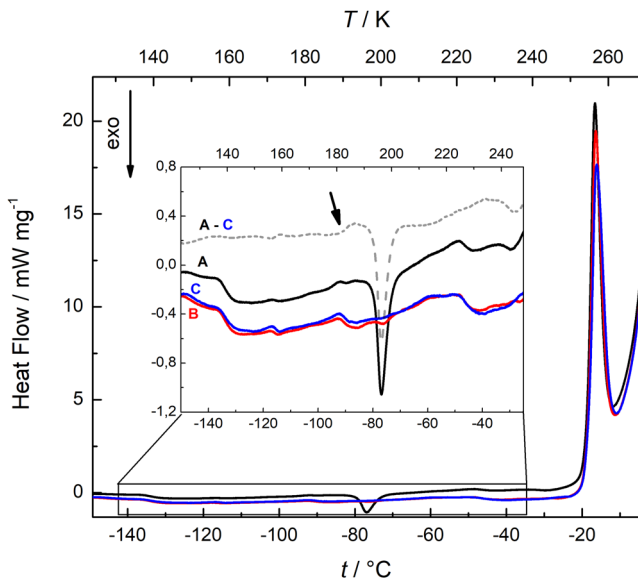


FIG. 4. The DSC heating scan (for the rate of 30 K min^{-1}) characterizing the 0.06M NaCl solution after freezing at the cooling rates of 100 K min^{-1} (A), 20 K min^{-1} (B), and 5 K min^{-1} (C). The inset with 6-fold magnification details the exothermic peak with the minimum at $\sim 197 \text{ K}$. The dashed gray curve then shows the difference between the A and C curves. The onset of the glass-to-liquid transition at 182 K is pointed out by the black arrow.

discussion, we assign the peak with the minimum at $\sim 197 \text{ K}$ to the cold crystallization of $\text{NaCl} \cdot 2\text{H}_2\text{O}$ from freeze-concentrated, vitrified solution. The absence of the cold crystallization event after cooling at 20 and 5 K min^{-1} then implies that vitrification does not occur at these rates in a measurable extent. To quantify the amounts of vitrified and crystallized eutectics, the areas of the peaks present in the thermograms are divided by the individual cooling rates in K s^{-1} and are listed in Table I. This procedure quantifies the enthalpy release at cold crystallization and the enthalpy uptake at eutectic melting, which is equivalent to the latent heat of fusion of $\text{NaCl} \cdot 2\text{H}_2\text{O}$.

Several 0.06M NaCl solutions with various room temperature pHs were prepared by adding HCl and NaOH solutions to yield lower and higher pHs, respectively. We measured their DSC heating scans to determine whether the area of the exothermic peaks at a peak minimum temperature of 197 K relates to the initial pHs of the solutions. Figure S4 of the [supplementary material](#) shows the measured heating scans with the indicated room temperature pHs, confirming the presence of a cold crystallization exothermic peak for all the samples. The dependence of the integrated area of the 197 K crystallization peak on the pH is plotted in Fig. S5 of the [supplementary material](#) and compared with the area of the eutectic melting peak at 252 K . It is obvious from the data that the vitrification and cold crystallization events do not depend on the acidity in 4 – 9 pH range. Rather than that it seems that minor variations in the cooling process beyond our control (e.g., impurities or fluctuations in the cooling rate) determine the scatter in this graph. For $\text{pH} < 4$, the area of the eutectic melting peak decreases significantly, whereas the area of the cold crystallization peak increases. This points out to a suppression of crystallization and enhancement of vitrification upon cooling NaCl solutions in an acidic environment. To make this case stronger, further experiments need to be done in future.

Heating the 3.42 mM NaCl solution

Figures S6 and S7 of the [supplementary material](#) display the DSC heating scans of the 3.42 mM NaCl solution. Similarly, to the corresponding scans for the 0.06M NaCl solution, the heating scans show the main endothermic peaks at around 273 K and 253 K , which relate to the consumed heat needed to melt the hexagonal ice and the heat required for melting the sodium chloride and hexagonal ice eutectic mixture, respectively. The $\text{NaCl} \cdot 2\text{H}_2\text{O}$ crystallization heat at $\sim 197 \text{ K}$ was detected for the rapidly cooled sample (Figs. S7 and S8 of the [supplementary material](#), the black curves). Again, to compare the heating scan with that of the 0.06M NaCl solution, the 0.06M NaCl scan (Fig. 4, the black curve) divided by the concentration correction factor of 17.5 ($0.06/0.00342$) is plotted as the red dotted line in Fig. S8 of the [supplementary material](#). The areas of the peaks divided by the heating rate present in the thermograms upon heating the frozen NaCl solution cooled by 100 K min^{-1} for the two NaCl concentrations (0.06M and 3.42 mM) are listed in Table I. Interestingly, the areas given in Table I do not scale with the concentration. While the concentration increases by a factor of 17.5 , the area of eutectic melting peak increases by a factor of 27 , but the area of cold crystallization increases only by a factor of 10 . In other words, in the more dilute 3.42 mM solution, cold crystallization is enhanced compared to the 0.06M solution, whereas formation of the eutectic

TABLE I. The areas of the peaks of eutectic melting (onset temperature at 252 K in Fig. 4 and Fig. S6) and cold crystallization (the onset temperature at 190 K in Fig. 4 and 193 K in Fig. S7) upon heating the frozen NaCl solution at 30 K min^{-1} that were first cooled at 100 K min^{-1} and upon heating of the ice spheres frozen by spraying the solution into the liquid nitrogen (Fig. 5). n = number of independent measurements.

	Areas of the peaks			
	Eutectic melting		Cold crystallization	
	0.06M NaCl	3.42 mM NaCl	0.06M NaCl	3.42 mM NaCl
Cooling 100 K min^{-1}	$(108.0 \pm 4.3) \text{ mJ mg}^{-1}$ $n = 4$	$(4.00 \pm 0.24) \text{ mJ mg}^{-1}$ $n = 2$	$(6.05 \pm 0.53) \text{ mJ mg}^{-1}$ $n = 4$	$(0.59 \pm 0.03) \text{ mJ mg}^{-1}$ $n = 2$
Ice spheres	$(9.2 \pm 3.8) \text{ mW s}$ $n = 2$...	$(1.3 \pm 0.5) \text{ mW s}$ $n = 2$...

is enhanced in the more concentrated 0.06M solution. The amounts of cold crystallization relative to the eutectic melting equal to 5% and 12% for the 0.06M and 3.42 mM solutions, respectively.

Ice spheres

In the case of heating the cold-loaded ice spheres prepared from 0.06M NaCl solution, loaded at 100 K, and heated at 30 K min^{-1} , the exothermic peak having the minimum at 197 K appears too (Fig. 5). The areas of peaks are given in Table I. As we did not weigh the ice spheres, the absolute areas in Fig. 5 cannot be compared to those in Fig. 4. The relative amount of cold crystallization heat to eutectic melting is 12%.

Change of the pH in BCP-dyed solutions

Ice samples resembling those utilized for the calorimetry measurement were also studied in terms of pH changes. The normalized

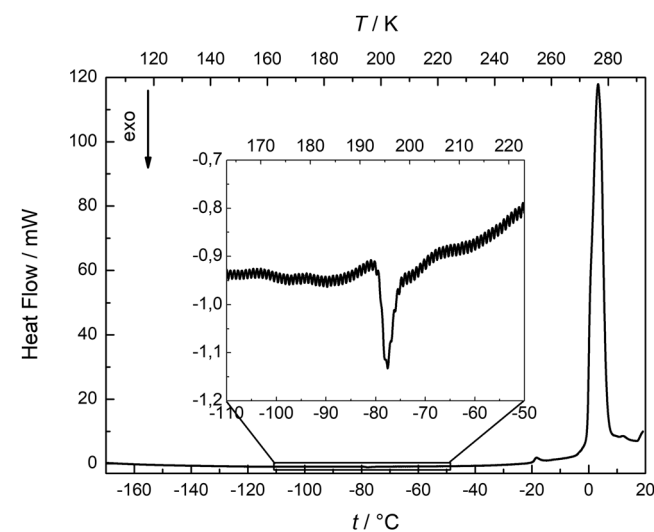


FIG. 5. The DSC heating scan (for the rate of 30 K min^{-1}) characterizing the 0.06M NaCl solution frozen in the liquid nitrogen into the form of ice spheres, with a detail (77-fold magnification) of the exothermic peak at $\sim 197 \text{ K}$.

absorption spectra of the BCP from the solution of 0.06M NaCl, with the $3.70 \times 10^{-6}\text{M}$ BCP indicator frozen by immersing the cuvette into liquid nitrogen, are shown in Fig. 6. The spectrum of a solution with an electrode-measured pH (6.20 ± 0.02) at room temperature (the black curve) exhibits two bands having their maxima at 434 and 587 nm; these maxima correspond to those of the acidic and the basic forms of the indicator, respectively. The computed room temperature $\text{H}_2\text{-}$ value of (6.042 ± 0.004) for $n = 3$ marginally varies from the pH potentiometrically determined by using a glass electrode. As we focus on the relative acidity changes, we do not attempt to eliminate this discrepancy, which most likely arises from the uncertainty of the indicator pK_a value at the given ionic strength. In the spectra measured immediately after freezing the sample in the liquid nitrogen (84–137 K, the red curve), increased intensity of the peak at 587 nm can be observed, indicating higher basicity upon cooling to

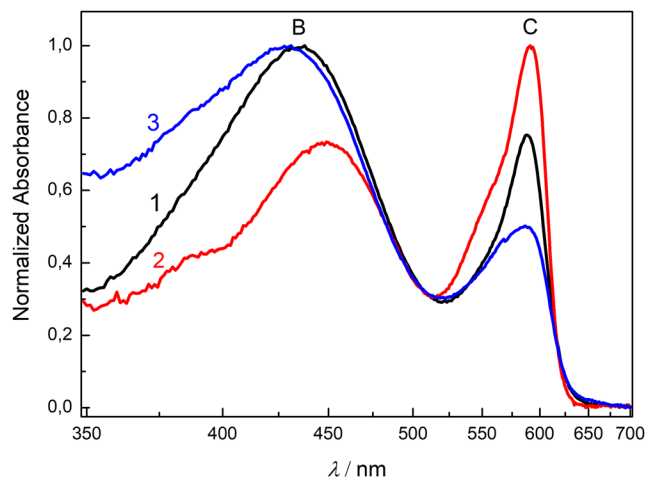


FIG. 6. The normalized UV-visible absorption spectra of the BCP ($c = 3.70 \times 10^{-6}\text{M}$) in the 0.06M NaCl solution, measured at various temperature intervals. First, the black curve (1) was recorded at room temperature; subsequently, we recorded the red curve (2) after immersing the cuvette in the liquid nitrogen at 84 K–137 K; and, finally, the blue curve (3) was captured after heating the cuvette to 221 K–234 K. The absorption peaks B and C correspond to the protonated and deprotonated forms of the BCP, respectively.

the H_{2-} value of (6.67 ± 0.01) for $n = 3$. After subsequent heating of the sample to 221 K (the blue curve), the intensity of the absorption band of the basic form at 587 nm decreases while the intensity of the acidic form rises, leading to the H_{2-} value of (6.27 ± 0.04) for $n = 3$. The same trend in increasing the H_{2-} value was observed in the quench freezing procedure carried out by spraying the 0.06M solution into the liquid nitrogen (the ice spheres), as presented in Fig. S9 and Table S1 of the [supplementary material](#). The 0.06M NaCl solution slowly cooled down from RT to 253 K exhibited a rise in the H_{2-} value by (0.23 ± 0.02) for three independent samples (data not shown). In the less concentrated sample (3.42 mM), no significant changes of the H_{2-} values were observed after cooling and subsequent heating.

Change of the pH in CR-dyed solutions

The absorption spectra of the CR indicator in the 0.06M NaCl solution are shown in Fig. S10 of the [supplementary material](#). The spectrum of the sample measured at room temperature (the black curve) with the computed initial H_{2-} value of 6.32 comprised only the neutral form B. After the sample was frozen in the liquid nitrogen, the intensity of the basic form increased, as in the case of the BCP solution. The H_{2-} value has increased to 7.05 following the quench in the liquid nitrogen. During the heating, the peak of the basic form gradually disappeared. The most pronounced decrease of the C form appeared above 218 K, with the H_{2-} value decreasing to 6.50. The H_{2-} values of each temperature interval are summarized in Table S2 of the [supplementary material](#).

ESEM observation

The 0.06M NaCl solution, after freezing by immersing the cuvette into the liquid nitrogen, was examined at 223 K by using the environmental scanning microscope. Figure 7 displays the ice I_h surface (the darker background) with parallel lines of the crystallized $\text{NaCl} \cdot 2\text{H}_2\text{O}$ (pale to white). The lines presumably delineate ice grain boundaries forming parallel lamellae. The separation between the lamellae [Fig. 7(a)]—red arrow; Fig. 7(b)—yellow square highlights the grain boundary width.

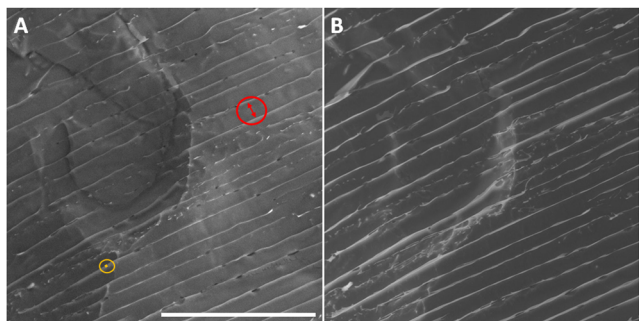


FIG. 7. The ESEM observation of the 0.06M NaCl liquid nitrogen-frozen solution observed at 223 K, using the backscattered electron (a) and secondary electron (b) detectors. The images indicate the hexagonal ice (dark gray) crystals and the grain boundaries (bright gray). The $200 \mu\text{m}$ scale is represented by the white bar; the red arrow shows the width of the ice lamella, and the yellow square highlights the grain boundary width.

Fig. S11 of the [supplementary material](#)] and the grain boundary width [Fig. 7(a)—yellow square; Fig. S12 of the [supplementary material](#)] was established to be $(18.24 \pm 0.77) \mu\text{m}$ and $(2.46 \pm 0.24) \mu\text{m}$, respectively; the interval provides information about the mean value and the standard deviation of the mean (Table S3 of the [supplementary material](#)). We performed 11 distance measurements; the obtained lamellae widths are shown in Fig. S11 of the [supplementary material](#), and a zoomed-in detail of the grain boundary width is provided in Fig. S13 of the [supplementary material](#).

DISCUSSION

Vitrified solutions were previously formed by combining the following factors: (1) very fast cooling (hyperquenching), (2) confining media, and (3) concentrated solutions of specific salts. The veins and lamellae with an FCS in between the crystals of pure hexagonal ice formed upon freezing a sodium chloride solution satisfy each of the above preconditions to some extent; thus, in these structures, the propensity to vitrification is reasonably expectable. The vitrification of solutions in the veins was already reported for, *inter alia*, minerals⁸⁰ and ice I_h containing sulfuric acid,⁴⁶ ammonium sulfate,⁸¹ citric acid, sugars,^{42,82} and other bulking agents applied in pharmaceutical freezing.^{83,84}

Even the fast freezing of NaCl solutions via cooling at 100 K min^{-1} or spraying the samples into liquid nitrogen does not lead to bulk vitrification. In this respect, NaCl solutions differ from others, such as the concentrated LiCl ones, where the cooling rate of approximately 90 K min^{-1} produces bulk vitrified glass.²³ Thus, considering all the cooling rates employed in our experiments, the most significant contribution to the heat exchange consists in the crystallization of ice I_h , which leaves behind a eutectic mixture to form an FCS in between the ice crystals as well as in the grooves and pools on the surfaces.³⁵ The result agrees with the outcomes of previous attempts to spray a NaCl solution into liquid nitrogen, allowing observation of primary ice veins.⁴⁷ The maximum volume of 22 w/w% NaCl solution hitherto found to fully vitrify upon plunge-cooling (dropping into liquid nitrogen on a Cu holder) was 10 nl.²⁴

All of our ESEM observations of the interior of ice samples frozen in liquid nitrogen reveal lamellar arrangement of ice intercalated with brine (Fig. 7). The spacing between the individual lamellae is almost completely regular, enabling us to calculate the average ice width, namely, $(18.24 \pm 0.77) \mu\text{m}$, $n = 11$. Similar structural patterns occur in sea ice.^{5,85–88} The structures formed from freezing solutions are known to be influenced by the salt identity and concentration, thermal gradients, and, hence, the freezing rate.^{36,89,90} Regrettably, our current microscopic setup does not allow examining the sample at temperatures low enough to support the observation of the vitrified solution below 180 K. The structures obtained after warming the sample from 77 K to 223 K nevertheless facilitate a detailed investigation of the crystallized eutectics (Fig. S12 of the [supplementary material](#)), whose average width corresponds to $(2.46 \pm 0.24) \mu\text{m}$, $n = 11$. Even though we took all the necessary precautions to acquire the micrographics as swiftly as possible, it cannot be excluded that these structures had undergone some metamorphism before being observed.

An unambiguous proof of the vitrification of a portion of the sample is deducible from the changed behavior of the sample in

the DSC, depending on the cooling rate. Only the fastest cooling rates applied (100 K min^{-1} or spraying the solution into liquid nitrogen) allow a small but notable and reproducible heat capacity change during the cooling and heating, with the onset temperatures of $\sim 200\text{ K}$ and $\sim 193\text{ K}$, respectively; at the same time, we also observe hydrohalite cold crystallization from the vitrified FCS at 197 K in the heating process. Such transitions are clearly visible in the 0.06M NaCl (Fig. 2) and still discernible in the 3.42 mM solutions (Figs. S2, S3, S7, and S8 of the [supplementary material](#)). We can thus infer that vitrification occurs, in the very least, at these concentrations and cooling rates. In the 3.42 mM solution, both the DSC and the dye indicators yield only small signals, suggesting that the concentration is at the very limit of the methods' sensitivity. The absence of the eutectic peak during the slow cooling procedure in the 3.42 mM NaCl solution (Fig. S1 of the [supplementary material](#)) most probably results from the sensitivity issue too, especially as the eutectic peak is well represented in the heating thermogram (Fig. S6 of the [supplementary material](#)). Cooling rates slower than 100 K min^{-1} do not produce significant signs of glass formation; we, therefore, suppose that either the eutectic had crystallized fully or the vitrified amount remained below detection. Previously, microemulsion freezing had enabled observation of the supposed T_g at $\sim 150\text{ K}$ in an emulsified solution at pressures above 100 MPa .²¹ This value ranges much lower than that of the crystallization peak of $\text{NaCl}\cdot 2\text{H}_2\text{O}$. Some transition at $\sim 150\text{ K}$ is also found in our samples frozen at atmospheric pressure (Fig. 4); however, the relevant intensity is small, and we observe the same effect in the slowly frozen samples. To the best of our knowledge, the NaCl vitrification temperature during cooling has not been characterized and reported thus far. We report here the vitrification onset for the FCS at $200\text{--}205\text{ K}$. The $\text{NaCl}\cdot 2\text{H}_2\text{O}$ crystallization temperature upon heating a vitrified NaCl solution at 197 K , as established within our experiments, corresponds well to that reported for hyperquenched NaCl solutions at 194 K .²⁷ The small difference in the onset temperatures, 197 K in our case and 194 K in the experiments conducted by Hallbrucker and Mayer, can be explained by varied warming rates; these equaled 30 K min^{-1} and 10 K min^{-1} , respectively.²⁷

In this context, our thermograms show the T_g of the transition at $\sim 200\text{ K}$ and $\sim 193\text{ K}$ for the cooling and the heating, respectively, because these transitions are significantly more pronounced in fast-cooled samples. The T_g values find relevant support not only in the literature^{27,32} but also the fact that the glass-to-liquid transition closely precedes the crystallization of $\text{NaCl}\cdot 2\text{H}_2\text{O}$. The assignment is also consistent with the recent observation that heating amorphous NaCl solutions at ambient pressure facilitates the generation of I_c at 160 K as well as the ice transformation to I_h with concomitant appearance of $\text{NaCl}\cdot 2\text{D}_2\text{O}$ at 185 K ; the entire procedure was recently studied via neutron diffraction.³⁰

Previous experiments involving the heating of hyperquenched salt solutions produced three devitrification peaks besides the crystallization of $\text{NaCl}\cdot 2\text{H}_2\text{O}$.²⁷ These peaks were assigned to distinct devitrification processes: water in the vicinity of chloride anions (159 K), pure water (165 K), and water surrounding sodium cations (181 K).²⁷ The ratio of these peaks was found to be characteristic of particular concentrations. The absence of such distinct peaks in our thermograms may be indicative of a local concentration higher

than those examined within the discussed experiments (4.6M corresponding to the eutectic concentration), also because the two lower-temperature crystallization peaks were reported to decrease their intensities with increasing concentration, relatively to the hydrohalite crystallization peak. Thus, we can infer from both the single devitrification peak and the other DSC thermogram signals that the fast freezing process in the hexagonal ice veins allows the NaCl concentration to reach the eutectic or even higher concentrations. For pure water, the T_g is 136 K , and for subeutectic $\text{NaCl}\cdot \text{H}_2\text{O}$ solutions, the T_g increases above 2 mol. \% (see Fig. 7 of Ref. 91) toward higher temperatures. At the eutectic concentration $\sim 9\text{ mol. \%}$ the T_g reaches $\sim 160\text{ K}$. The $T_g \sim 200\text{ K}$ observed in Fig. 2 is only possible for solutions clearly exceeding the eutectic concentration. A similar situation is well documented in other solutes, including sucrose. In this case, the T_g of the eutectic solution is 190 K , but the maximally freeze concentrated solution shows a T_g of 230 K .^{92,82} The other conclusion drawn from the absence of the three crystallization peaks observed previously in the thermograms concerns the presence of a homogeneous solution, namely, the one that leaves no space for individual ion domains.

In the NaCl glass devitrification, the solution formed before the $\text{NaCl}\cdot 2\text{H}_2\text{O}$ crystallized. The glass-to-liquid transition is deduced from the appearance of the endotherm with the onset at 182 K , best noticeable in the difference thermogram (the dashed gray curves in Figs. 4 and Fig. S7 of the [supplementary material](#)). Such true glass transition (as opposed to devitrification, where the amorphous phase changes into the crystalline one, avoiding the liquid phase) is typical of hyperquenched water and salt solutions.^{27,93} A crystallization event upon heating is termed "cold crystallization" and arises from the growth into crystals of nuclei that did not have enough time to complete the process during cooling. Usually, these nuclei are trapped in a glassy matrix, which is then consumed by the growth of the crystals; in other words, cold crystallization upon heating implies vitrification upon cooling, with some crystallization nuclei forming already upon cooling. The nuclei typically remain kinetically stable in the glassy matrix; however, as soon as the glass devitrifies upon heating, the crystal growth begins, starting from the nuclei. Such an interpretation is strongly supported by the observed devitrification transition, marked by the black arrow right before the cold crystallization event in Fig. 4. The other peaks (not discussed herein) present in the heating thermograms (Fig. 4) for all of the cooling temperatures appear to be characteristic and reproducible; however, their corresponding heats are very small, approaching the baseline drift, and therefore we do not interpret them.

The reason for glass formation in a portion of the eutectic can be sought in the limited dimensions of the veins; during our microscopic examination, the upper dimension limit has never exceeded several micrometers. The freezing temperatures of bulk and emulsified NaCl solutions were previously observed at 236 and 188 K , respectively.⁹⁴ Thus, it is well conceivable that at high cooling rates a portion of the eutectic solution in the ice veins does not crystallize before reaching 200 K ; in these conditions, the brine viscosity increases to such an extent that crystallization is inhibited.⁹⁵ The vitrification of a NaCl solution was already observed in nanoporous silica glass by Zhao, Pan, Cao, and Wang,³² who used the cooling rate of 20 K min^{-1} . The authors argued that the pure ice

crystallized in the center of the pores had expelled the solution to the sides, concentrating it to the eutectic composition; the two events together then rendered the solution prone to glass formation. In the paper of Zhao *et al.*, devitrification and $\text{NaCl} \cdot 2\text{H}_2\text{O}$ crystallization were observed only with some combinations of NaCl concentrations and pore diameters; the T_g gradually decreased from 178 K to 160 K in 54 nm and 2.6 nm pores, respectively. Thus, the T_g value established within our research (ca. 182 K) places the confinement dimension above 54 nm and stands close to the T_g of the bulk solution formed by hyperquenching.

In ice I_h , we can expect the dimensions of the veins inside the bulk ice to be smaller than those of the ice boundary grooves observed on the surface. Moreover, it cannot be excluded that some small structures collapsed into larger ones when evaporating in the microscope. With the current observations, we cannot determine if vitrification occurs only in the smallest veins in between the I_h crystals or partly in channels of all dimensions.

The extent of vitrification as compared to eutectic crystallization is not easily definable from our data. The straightest quantification could be performed by comparing the eutectic crystallization heat with that of the liquid-to-glass, glass-to-liquid, or NaCl cold crystallization processes. Regrettably, the eutectic crystallization heat is not available to the 100 K min⁻¹ cooling experiment because it is hidden under the ice crystallization curve. The heating thermograms offer well-separated eutectic melting peaks for all of the cooling rates; the peaks, however, contain the contributions of both the heats from the originally crystallized eutectics and the initially vitrified (but crystallized in the course of heating) part of the sample. The amounts of the heat released during the cold crystallization of NaCl equal only 5%, 12% and 12% of the heat needed for the eutectic melting in the 0.06M and 3.42 mM NaCl solutions and 0.06M ice sphere, respectively. To quantify the ratio of the vitrified solution compared to that of the eutectic melt, we utilized the previously determined latent heat of the eutectic mixture (233.0 ± 1.6) J g⁻¹^{94,96,97} and estimated the enthalpy change of the reaction $\text{NaCl}_{(\text{aq})} + 2 \text{H}_2\text{O}_{(\text{l})} \leftrightarrow \text{NaCl} \cdot 2\text{H}_2\text{O}_{(\text{s})}$ to -192.12 J g⁻¹. Thus, we obtained (6.8% ± 0.6%) and (17.9% ± 1.5%) of the vitrified solution in the total amount of the melting eutectics for the 0.06M and 3.42 mM NaCl solutions cooled at rate of 100 K min⁻¹, respectively. The enthalpy change of the above reaction was estimated from the 298-K standard molar enthalpies of the formation of $\text{NaCl}_{(\text{cr})}$ (-411.27 kJ mol⁻¹), $\text{NaCl} \cdot 2\text{H}_2\text{O}_{(\text{cr})}$ (-997.24 kJ mol⁻¹)⁹⁸ and water -285.82 kJ mol⁻¹; in the estimation process, we also employed the dissolution enthalpy of NaCl in water 3.88 kJ mol⁻¹⁹⁹. The current experiments do not explain the higher relative amount of vitrified salt observed in the lower concentration. The occurrence of a higher amount of vitrified salt in the ice spheres (12%) as compared to the 100 K min⁻¹ cooling (5%) is most probably due to the higher freezing rate. We do not establish a clear dependence between the initial solution acidity and the extent of vitrification (Fig. S5 of the [supplementary material](#)). However, it seems that at pH < 4, the tendency to vitrify is enhanced. At the current stage, we cannot determine whether this observation is related to the enhanced concentration of the Cl^- ions from the HCl responsible for the solution acidification.

The occurrence of thermodynamically unstable crystal modifications was previously caused by freezing in small volumes; principally, halite was found to be formed instead of hydrohalite,¹⁰⁰ and

letovicite II substituted letovicite III²⁸ in the freezing of NaCl and ammonium sulfate solutions, respectively. Conversely, slow crystallization from a NaCl saturated solution produced hydrohalite at -15 °C.¹⁰¹ Our study records the formation of the thermodynamically unstable glass state. Locating the onsets of the eutectic melting peaks to 252 K is consistent with the eutectic point at 252 K for water $\text{NaCl} \cdot 2\text{H}_2\text{O}$ (hydrohalite).¹⁰² This value suggests that the presented eutectic freezing and also cold crystallization allow the formation of the thermodynamically more stable hydrohalite from the FCS. Contrarily to the observations by Drebushchak, Ogienko and Yunoshev,⁷⁹ our thermograms do not indicate around 245 K a reproducible signal corresponding to halite crystallization;^{79,103} the explanation may consist in the heating scan being 10 times faster than that applied by Drebushchak *et al.*

As NaCl is the salt of strong monovalent acid and base, neither its concentration increase nor its crystallization is expected to change the pH in the veins of the FCS. The only option to explain the observed pH change effects rests in the unequal distribution coefficients of the sodium cation and the chloride anion between the ice and the freeze concentrated solution. In this context, the Workman-Reynolds potentials between ice and freeze concentrated NaCl solutions were previously measured by multiple researchers,^{54,104–107} and the subsequent acidity change was observed either by using sulfonephthalein indicators or indirectly via a hydrolytic reaction.^{49,53,108} All of the experiments performed to date suggest that chloride anions incorporate into ice much more frequently than sodium cations. These uneven distribution coefficients between ice and freeze-concentrated solutions were recently confirmed via molecular dynamic simulation;¹⁰⁹ the procedure showed that a chloride anion can substitute two water molecules in the crystal lattice of ice, whereas sodium cations enter interstitial positions. The absolute value of the distribution coefficient for the chloride (and any other) ion remains essentially unknown.^{5,7,19} Due to the low concentrations in ice and possible surface accumulation, only two indirect methods for determining ion concentrations in bulk ice are available. One of the techniques stems from dielectric spectroscopy measurement, suggesting that the concentration of HCl in ice reaches approximately 10⁻⁵ M but is certainly not higher than 10⁻⁴ M.¹¹⁰ In the same concentration range, the value of (7 × 10⁻⁵ M) is based on the other approach, namely, measuring the shear stress curves for the ice monocrystals grown out of an HCl solution.¹¹¹ To the best of our knowledge, the value of NaCl solubility in ice has not been determined thus far.

Our observed acidity drop in fast frozen solutions, however, corresponds to the preferential incorporation of chloride anions into the ice. The sulfonephthalein indicators are certainly too large to be incorporated into the ice lattice; thus, they will be concentrated into the eutectic FCS during the freezing process. The crystallization of the eutectic would place the indicator onto the surfaces of the hydrohalite and/or ice crystals. If a vitrified glass solution is formed, the indicator can be inside it. The acidity change due to the neutralized Workman-Reynolds potential was more significant for the rapid than the slow cooling ($\Delta\text{H}_2^- \sim 0.6$ and 0.2, respectively); however, the effect invariably increased the basicity. The amount of ions incorporated into the ice and thus also the apparent acidity change in the veins depend on the counter ions and the freezing dynamics regulated by the freezing rate. It should be noted that our observations of a more prominent acidity increase occurring at a high

cooling rate rather than a slow one stand in contrast with the predictions by Bronshteyn and Chernov¹⁰⁸ and Sola and Corti.¹⁰⁴ Further experiments, however, are needed to reconcile the observations with the theoretical model. In the heating process, acidity changes are observed prevalently above the T_g . We can only speculate on the cause of these changes; the most plausible explanation seems to consist in the diffusion of HCl out of the ice. The pH variations observed during the freezing cannot be attributed to an increased concentration of CO₂ and its dissolution in the veins because our experiments using solutions saturated with N₂ showed the same trend as those in equilibrium with the air (data not shown).

CONCLUSION

Previously, spatial confinement to impede crystallization while enhancing vitrification was materialized in micelles, suspensions, nanoporous glass, and clay. We propose that the confinement in ice I_h veins can serve the same purpose. During the rapid freezing (100 K min⁻¹) of an aqueous NaCl solution, ice I_h forms; subsequently, a part of the eutectic mixture crystallizes and another small portion turns into glass. The acidity decrease accompanying the freezing process is consistent with preferential incorporation of chloride anions into the ice as compared to sodium cations. In the heating process, we observe the glass transition into the liquid state, followed by NaCl · 2H₂O cold crystallization and the resulting acidity increase. The method of glass vitrification in ice I_h veins upon fast cooling can be used to study the corresponding process in aqueous solutions, which until now was assumed to require hyperquenching techniques.

SUPPLEMENTARY MATERIAL

See [supplementary material](#) for discussed figures and tables.

ACKNOWLEDGMENTS

This work was supported by the Czech Science Foundation (Grant No. 19-08239S). T.L. gratefully acknowledges funding by the Austrian Research Agency FFG (project EARLYSNOW) and the Austrian Science Fund (FWF) (Project No. I1392).

The authors declare that they have no conflict of interest.

REFERENCES

- ¹V. Fuentes-Landete, C. Mitterdorfer, P. H. Handle, G. N. Ruiz, J. Bernard, A. Bogdan, M. Seidl, K. Amann-Winkel, J. Stern, F. Stephan, and T. Loerting, in *Proceedings of the International School of Physics “Enrico Fermi” Course 187: Water: Fundamentals as the Basis for Understanding the Environment and Promoting Technology*, edited by P. G. Debenedetti, M. A. Ricci, and F. Bruni (IOS, Amsterdam; SIF, Bologna, 2015), pp. 2173–2208.
- ²P. H. Handle, T. Loerting, and F. Sciotino, *Proc. Natl. Acad. Sci. U. S. A.* **114**(51), 13336–13344 (2017).
- ³P. G. Debenedetti and H. E. Stanley, *Phys. Today* **56**(6), 40–46 (2003).
- ⁴A. C. A. Boogert, P. A. Gerakines, and D. C. B. Whittet, *Annu. Rev. Astron. Astrophys.* **53**(1), 541–581 (2015).
- ⁵V. F. Petrenko and R. W. Whitworth, *Physics of Ice* (Oxford University Press, Oxford, 1999).
- ⁶P. Gallo, K. Amann-Winkel, C. A. Angell, M. A. Anisimov, F. Caupin, C. Chakravarty, E. Lascaris, T. Loerting, A. Z. Panagiotopoulos, J. Russo, J. A. Sellberg, H. E. Stanley, H. Tanaka, C. Vega, L. Xu, and L. G. M. Pettersson, *Chem. Rev.* **116**(13), 7463–7500 (2016).
- ⁷T. Bartels-Rausch, H. W. Jacobi, T. F. Kahan, J. L. Thomas, E. S. Thomson, J. P. D. Abbott, M. Ammann, J. R. Blackford, H. Bluhm, C. Boxe, F. Domine, M. M. Frey, I. Gladich, M. I. Guzmán, D. Heger, T. Huthwelker, P. Klán, W. F. Kuhs, M. H. Kuo, S. Maus, S. G. Moussa, V. F. McNeill, J. T. Newberg, J. B. C. Pettersson, M. Roeselová, and J. R. Sodeau, *Atmos. Chem. Phys.* **14**(3), 1587–1633 (2014).
- ⁸T. Bartels-Rausch, *Nature* **494**(7435), 27–29 (2013).
- ⁹B. Zobrist, C. Marcolla, D. A. Pedernera, and T. Koop, *Atmos. Chem. Phys.* **8**(17), 5221–5244 (2008).
- ¹⁰A. Virtanen, J. Joutsensaari, T. Koop, J. Kannisto, P. Yli-Pirila, J. Leskinen, J. M. Makela, J. K. Holopainen, U. Poschl, M. Kulmala, D. R. Worsnop, and A. Laaksonen, *Nature* **467**(7317), 824–827 (2010).
- ¹¹J. Dubochet and A. W. McDowall, *J. Microsc.* **124**(3), 3–4 (1981).
- ¹²M. Adrian, J. Dubochet, J. Lepault, and A. W. McDowall, *Nature* **308**(5954), 32–36 (1984).
- ¹³J. Dubochet and E. Knapek, *PLoS Biol.* **16**(4), e2005550 (2018).
- ¹⁴R. S. Dillard, C. M. Hampton, J. D. Strauss, Z. Ke, D. Altomara, R. C. Guerrero-Ferreira, G. Kiss, and E. R. Wright, *Microsc. Microanal.* **24**(4), 406–419 (2018).
- ¹⁵P. Bruggeller and E. Mayer, *Nature* **288**(5791), 569–571 (1980).
- ¹⁶E. Mayer, *J. Appl. Phys.* **58**(2), 663–667 (1985).
- ¹⁷D. Heger, J. Jirkovsky, and P. Klan, *J. Phys. Chem. A* **109**(30), 6702–6709 (2005).
- ¹⁸J. R. Blackford, *J. Phys. D: Appl. Phys.* **40**(21), R355–R385 (2007).
- ¹⁹P. V. Hobbs, *Ice Physics* (Oxford University Press, Oxford, 2010).
- ²⁰S. Klotz, L. E. Bove, T. Strässle, T. C. Hansen, and A. M. Saitta, *Nat. Mater.* **8**, 405 (2009).
- ²¹H. Kanno and C. A. Angell, *J. Phys. Chem.* **81**(26), 2639–2643 (1977).
- ²²G. N. Ruiz, K. Amann-Winkel, L. E. Bove, H. R. Corti, and T. Loerting, *Phys. Chem. Chem. Phys.* **20**, 6401–6408 (2018).
- ²³C. A. Angell and E. J. Sare, *J. Chem. Phys.* **52**(3), 1058–1068 (1970).
- ²⁴V. Berejnov, N. S. Husseini, O. A. Alsaeid, and R. E. Thorne, *J. Appl. Crystallogr.* **39**(2), 244–251 (2006).
- ²⁵M. Warkentin, J. P. Sethna, and R. E. Thorne, *Phys. Rev. Lett.* **110**(1), 015703 (2013).
- ²⁶A.-A. Ludl, L. E. Bove, J. Li, M. Morand, and S. Klotz, *Eur. Phys. J.: Spec. Top.* **226**(5), 1051–1063 (2017).
- ²⁷A. Hallbrucker and E. Mayer, *J. Phys. Chem.* **92**(7), 2007–2012 (1988).
- ²⁸B. J. Murray and A. K. Bertram, *Phys. Chem. Chem. Phys.* **10**(22), 3287 (2008).
- ²⁹R. Bergman and J. Swenson, *Nature* **403**, 283 (2000).
- ³⁰A. A. Ludl, L. E. Bove, A. M. Saitta, M. Salanne, T. C. Hansen, C. L. Bull, R. Gaal, and S. Klotz, *Phys. Chem. Chem. Phys.* **17**(21), 14054–14063 (2015).
- ³¹B. J. Murray, D. A. Knopf, and A. K. Bertram, *Nature* **434**, 202 (2005).
- ³²L. Zhao, L. Pan, Z. Cao, and Q. Wang, *Chem. Phys. Lett.* **647**, 170–174 (2016).
- ³³D. Cullen and I. Baker, *Microsc. Res. Tech.* **55**(3), 198–207 (2001).
- ³⁴D. Iliescu and I. Baker, *J. Glaciol.* **54**(185), 362–370 (2017).
- ³⁵J. Krausko, J. Runštuk, V. Neděla, P. Klán, and D. Heger, *Langmuir* **30**(19), 5441–5447 (2014).
- ³⁶L. Vetráková, V. Neděla, J. Runštuk, and D. Heger, *Cryosphere Discuss.* **2019**, 1–28.
- ³⁷J. Krausko, J. K. E. Malongwe, G. Bičanová, P. Klán, D. Nachtigallová, and D. Heger, *J. Phys. Chem. A* **119**(32), 8565–8578 (2015).
- ³⁸R. Kania, J. K. E. Malongwe, D. Nachtigallová, J. Krausko, I. Gladich, M. Roeselová, D. Heger, and P. Klán, *J. Phys. Chem. A* **118**(35), 7535–7547 (2014).
- ³⁹D. Heger and P. Klan, *J. Photochem. Photobiol., A* **187**(2–3), 275–284 (2007).
- ⁴⁰M. Thangswamy, P. Maheshwari, D. Dutta, V. Rane, and P. K. Pujari, *J. Phys. Chem. A* **122**(23), 5177–5189 (2018).
- ⁴¹A. Bogdan and M. J. Molina, *J. Phys. Chem. A* **121**(16), 3109–3116 (2017).
- ⁴²A. Bogdan, M. J. Molina, H. Tenhu, E. Bertel, N. Bogdan, and T. Loerting, *Sci. Rep.* **4**, 7414 (2014).
- ⁴³A. Bogdan, M. J. Molina, H. Tenhu, E. Mayer, and T. Loerting, *Nat. Chem.* **2**, 197 (2010).
- ⁴⁴J. Krausko, G. Ondrušková, and D. Heger, *J. Phys. Chem. A* **119**(43), 10761–10763 (2015).
- ⁴⁵G. Ondrušková, J. Krausko, J. N. Stern, A. Hauptmann, T. Loerting, and D. Heger, *J. Phys. Chem. C* **122**(22), 11945–11953 (2018).

- ⁴⁶C. McCarthy, J. R. Blackford, and C. E. Jeffree, *J. Microsc.* **249**(2), 150–157 (2013).
- ⁴⁷J. R. Blackford, C. E. Jeffree, D. F. J. Noake, and B. A. Marmo, *Proc. Inst. Mech. Eng., Part L* **221**(3), 151–156 (2007).
- ⁴⁸W. Rosenthal, J. Saleta, and J. Dozier, *Cold Reg. Sci. Technol.* **47**(1-2), 80–89 (2007).
- ⁴⁹D. Heger, J. Klanova, and P. Klan, *J. Phys. Chem. B* **110**(3), 1277–1287 (2006).
- ⁵⁰L. Vetráková, V. Vykoukal, and D. Heger, *Int. J. Pharm.* **530**(1-2), 316–325 (2017).
- ⁵¹N. Murase and F. Franks, *Biophys. Chem.* **34**(3), 293–300 (1989).
- ⁵²P. Sundaramurthy, E. Shalaev, and R. Suryanarayanan, *J. Phys. Chem. B* **114**(14), 4915–4923 (2010).
- ⁵³L. Krausková, J. Procházková, M. Klašková, L. Filipová, R. Chaloupková, S. Malý, J. Damborsky, and D. Heger, *Int. J. Pharm.* **509**(1-2), 41–49 (2016).
- ⁵⁴E. J. Workman and S. E. Reynolds, *Phys. Rev.* **78**(3), 254 (1950).
- ⁵⁵J. J. Li, K. Chatterjee, A. Medek, E. Shalaev, and G. Zografi, *J. Pharm. Sci.* **93**(3), 697–712 (2004).
- ⁵⁶J. Ju, J. Kim, L. Vetráková, J. Seo, D. Heger, C. Lee, H.-I. Yoon, K. Kim, and J. Kim, *J. Hazard. Mater.* **329**, 330–338 (2017).
- ⁵⁷Y. Choi, H.-I. Yoon, C. Lee, L. Vetráková, D. Heger, K. Kim, and J. Kim, *Environ. Sci. Technol.* **52**(9), 5378–5385 (2018).
- ⁵⁸L. M. Shulman, *Astron. Astrophys.* **416**(1), 187–190 (2004).
- ⁵⁹Y. Orii and M. Morita, *J. Biochem.* **81**(1), 163–168 (1977).
- ⁶⁰J. T. Newberg, *Fluid Phase Equilib.* **478**, 82–89 (2018).
- ⁶¹P. H. Gleick, *Water in Crisis. A Guide to the World's Fresh Water Resources* (Oxford University Press, 1993).
- ⁶²B. Light, R. C. Carns, and S. G. Warren, *J. Geophys. Res.: Oceans* **121**(7), 4966–4979, <https://doi.org/10.1002/2016jc011803> (2016).
- ⁶³S. G. Warren, *Philos. Trans. R. Soc. A* **377**(2146), 20180161 (2019).
- ⁶⁴D. A. Wiesenburg and B. J. Little, *Ocean Phys. Eng.* **12**(3-4), 127–165 (1988).
- ⁶⁵E. M. Knipping, M. J. Lakin, K. L. Foster, P. Jungwirth, D. J. Tobias, R. B. Gerber, D. Dabdub, and B. J. Finlayson-Pitts, *Science* **288**(5464), 301–306 (2000).
- ⁶⁶X. Yang, V. Neděla, J. Runstuk, G. Ondrušková, J. Krausko, L. Vetráková, and D. Heger, *Atmos. Chem. Phys.* **17**(10), 6291–6303 (2017).
- ⁶⁷A. Krepelova, T. Huthwelker, H. Bluhm, and M. Ammann, *ChemPhysChem* **11**(18), 3859–3866 (2010).
- ⁶⁸N. A. Gavrilenko, N. V. Saranchina, A. V. Sukhanov, and D. A. Fedan, *Mendeleev Commun.* **28**(4), 450–452 (2018).
- ⁶⁹W. Yao and R. H. Byrne, *Environ. Sci. Technol.* **35**(6), 1197–1201 (2001).
- ⁷⁰J. A. Dean, *Lange's Handbook of Chemistry*, 14th ed. (McGraw-Hill, New York, 1992).
- ⁷¹D. Perrin, *Aust. J. Chem.* **16**(4), 572–578 (1963).
- ⁷²M. M. Ghoneim, Y. M. Issa, and M. A. Ashy, *Indian J. Chem., Sect. A: Inorg., Bio-inorg., Phys., Theor. Anal. Chem.* **18**(4), 349–350 (1979).
- ⁷³L. P. Hammett and M. A. Paul, *J. Am. Chem. Soc.* **56**, 827–829 (1934).
- ⁷⁴L. P. Hammett and A. J. Deyrup, *J. Am. Chem. Soc.* **54**(7), 2721–2739 (1932).
- ⁷⁵R. Govindarajan, K. Chatterjee, L. Gatlin, R. Suryanarayanan, and E. Y. Shalaev, *J. Pharm. Sci.* **95**(7), 1498–1510 (2006).
- ⁷⁶D. L. Williams-Smith, R. C. Bray, M. J. Barber, A. D. Tsopanakis, and S. P. Vincent, *Biochem. J.* **167**(3), 593–600 (1977).
- ⁷⁷V. Nedela, *Microsc. Res. Tech.* **70**(2), 95–100 (2007).
- ⁷⁸V. Nedela, E. Tihlarikova, J. Runstuk, and J. Hudec, *Ultramicroscopy* **184**, 1–11 (2018).
- ⁷⁹V. A. Drebushchak, A. G. Ogienko, and A. S. Yunoshev, *Thermochim. Acta* **647**, 94–100 (2017).
- ⁸⁰G. Desbois, J. L. Urai, C. Burkhardt, M. R. Drury, M. Hayles, and B. Humbel, *Geofluids* **8**(1), 60–72 (2008).
- ⁸¹A. Bogdan, M. J. Molina, H. Tenhu, E. Mayer, E. Bertel, and T. Loerting, *J. Phys.: Condens. Matter* **23**(3), 035103 (2011).
- ⁸²A. Hauptmann, K. Podgoršek, D. Kuzman, S. Srčić, G. Hoelzl, and T. Loerting, *Pharm. Res.* **35**(5), 101 (2018).
- ⁸³B. S. Chang and C. S. Randall, *Cryobiology* **29**(5), 632–656 (1992).
- ⁸⁴E. Y. Shalaev, F. Franks, and P. Echlin, *J. Phys. Chem.* **100**(4), 1144–1152 (1996).
- ⁸⁵D. L. Anderson and W. F. Weeks, *Trans., Am. Geophys. Union* **39**(4), 632–640 (1958).
- ⁸⁶W. F. Weeks, *On Sea Ice* (University of Alaska Press, 2010), ISBN: 9781602231016.
- ⁸⁷D. N. Thomas, *Sea Ice* (Wiley-Blackwell, Chichester, UK, 2017).
- ⁸⁸K. Nagashima and Y. Furukawa, *J. Phys. Chem. B* **101**(32), 6174–6176 (1997).
- ⁸⁹P. K. Rohatgi and C. M. Adams, *J. Glaciol.* **6**(47), 663–679 (1967).
- ⁹⁰S. Maus, “Prediction of the cellular microstructure of sea ice by morphological stability theory,” in *Physics and Chemistry of Ice*, edited by W. Kuhs (Royal Society of Chemistry, 2007), pp. 371–382, ISBN: 978-1-84755-777-3.
- ⁹¹K. Hofer, G. Astl, E. Mayer, and G. P. Johari, *J. Phys. Chem.* **95**(26), 10777–10781 (1991).
- ⁹²B. Zobrist, V. Soonsin, B. P. Luo, U. K. Krieger, C. Marcolla, T. Peter, and T. Koop, *Phys. Chem. Chem. Phys.* **13**(8), 3514–3526 (2011).
- ⁹³G. P. Johari, A. Hallbrucker, and E. Mayer, *Nature* **330**, 552 (1987).
- ⁹⁴T. Koop, A. KapilaShrami, L. T. Molina, and M. J. Molina, *J. Geophys. Res.: Atmos.* **105**(D21), 26393–26402, <https://doi.org/10.1029/2000jd000413> (2000).
- ⁹⁵F. Franks, *J. Microsc.* **141**(3), 243–249 (1986).
- ⁹⁶B. Han, J. H. Choi, J. A. Dantzig, and J. C. Bischof, *Cryobiology* **52**(1), 146–151 (2006).
- ⁹⁷J. Leya, P. Losada-Pérez, C. Glorieux, and J. Thoen, *J. Therm. Anal. Calorim.* **129**(3), 1727–1739 (2017).
- ⁹⁸D. G. Archer, *J. Phys. Chem. Ref. Data* **21**(4), 793–829 (1992).
- ⁹⁹N. Hubert, R. Solimando, A. Pere, and L. Schuffenecker, *Thermochim. Acta* **294**(2), 157–163 (1997).
- ¹⁰⁰R. Wagner, O. Möhler, and M. Schnaiter, *J. Phys. Chem. A* **116**(33), 8557–8571 (2012).
- ¹⁰¹B. Light, R. E. Brandt, and S. G. Warren, *J. Geophys. Res.* **114**(C7), C07018, <https://doi.org/10.1029/2008jc005211> (2009).
- ¹⁰²L. Komunjer, M. Ollivon, B. Fouconnier, A. T. Luong, I. Pezon, and D. Clausse, *J. Therm. Anal. Calorim.* **98**(1), 125–131 (2009).
- ¹⁰³D. Clausse, I. Pezon, L. Potier, and S. Raynal, in *Thermodynamic Modeling and Materials Data Engineering*, edited by J.-P. Caliste, A. Truyol, and J. H. Westbrook (Springer Berlin Heidelberg, Berlin, Heidelberg, 1998), pp. 115–128.
- ¹⁰⁴M. I. Sola and H. R. Corti, *An. Asoc. Quim. Argent.* **81**(6), 483–498 (1993).
- ¹⁰⁵P. W. Wilson and A. D. J. Haymet, *J. Phys. Chem. B* **114**(39), 12585–12588 (2010).
- ¹⁰⁶P. W. Wilson and A. D. J. Haymet, *J. Phys. Chem. B* **112**(37), 11750–11755 (2008).
- ¹⁰⁷Z. Roubal, Z. Szabó, M. Steinbauer, D. Heger, and R. Kubásek, presented at the Progress in Electromagnetics Research Symposium, 2011.
- ¹⁰⁸V. L. Bronshteyn and A. A. Chernov, *J. Cryst. Growth* **112**(1), 129–145 (1991).
- ¹⁰⁹M. M. Conde, M. Rovere, and P. Gallo, *Phys. Chem. Chem. Phys.* **19**(14), 9566–9574 (2017).
- ¹¹⁰I. G. Young and R. E. Salomon, *J. Chem. Phys.* **48**(4), 1635–1644 (1968).
- ¹¹¹T. Nakamura and S. J. Jones, *Scr. Metall.* **4**(2), 123–126 (1970).
- ¹¹²H. W. Robinson, “The influence of neutral salts on the pH of phosphate buffers mixtures,” *J. Bio. Chem.* **82**, 775–802 (1929).
- ¹¹³C. Rottman, G. Grader, Y. De Hazan, S. Melchior, and D. Avnir, “Surfactant-induced modification of dopants reactivity in sol-gel matrixes,” *J. Am. Chem. Soc.* **121**(37), 8533–8543 (1999).